Supplementary Information (SI) for Journal of Materials Chemistry A.

Nitrogen-Rich Porous Carbon Electrocatalyst Derived from Supramolecular Polymer-Encapsulated Iron Precursors for Oxygen Reduction Reaction

Shufei Zhu [a, c, 1], Tao Wu [a, e, 1], Jia Liu [b, c], Hai Huang [a, c], Biaohuang Liu [a, c], Jiashen Meng [d, *] Yiming Xie [a, *], Canzhong Lu [b, c, *]

[a] Engineering Research Center of Environment-Friendly Functional Materials, Ministry of Education, Institute of Materials Physical Chemistry, Huaqiao University, Xiamen 361021, P.R. China

[b] CAS Key Laboratory of Design and Assembly of Functional Nanostructures, and Fujian Provincial Key Laboratory of Nanomaterials, Fujian Institute of Research on the Structure of Matter, Chinese Academy of Sciences, Fuzhou, Fujian 350002, P.R. China

[c] Xiamen Key Laboratory of Rare Earth Photoelectric Functional Materials, Center of Rare-earth Materials, Haixi Institutes, Chinese Academy of Sciences, Xiamen 361021, P.R. China

[d] School of Materials Science and Engineering, Wuhan University of Technology, Wuhan 430070, China

[e] Zhanjiang Health School of Guangdong, Zhanjiang 524037, P.R. China

[*]Corresponding Author: Yiming Xie, Jiashen Meng, Can-Zhong Lu

Email: ymxie@hqu.edu.cn, jsmeng@whut.edu.cn, czlu@fjirsm.ac.cn

[1] These authors contributed equally to this work.

CB7 solution **CB7&PAA** **Fc@CB7&PAA**

Figure S1. Photograph of the CB7 solution, CB7&PAA and Fc@CB7&PAA.

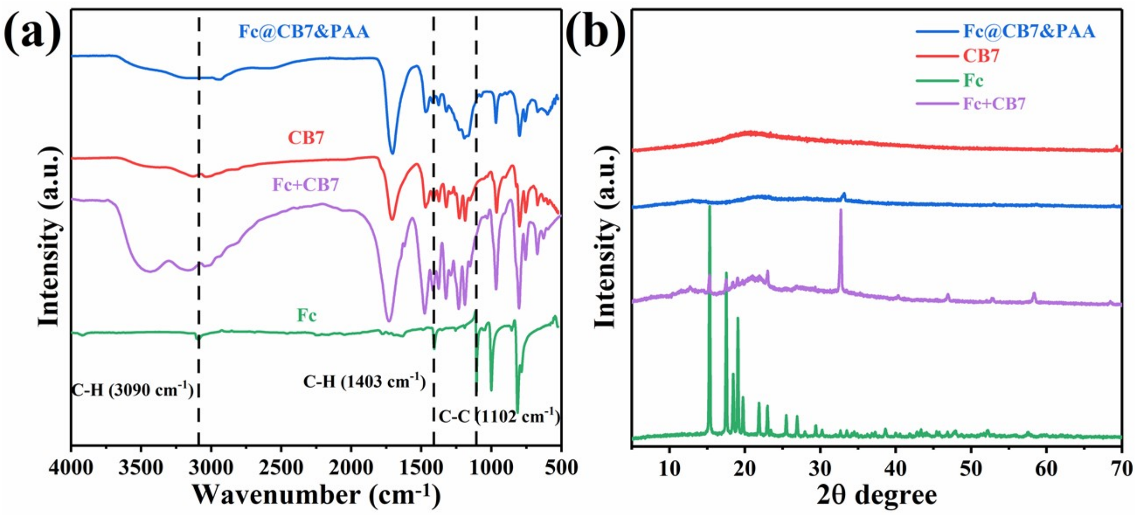

Figure S2. (a) IR spectra and (b) XRD spectra of Fc, CB7, Fc+CB7 and Fc@CB7&PAA

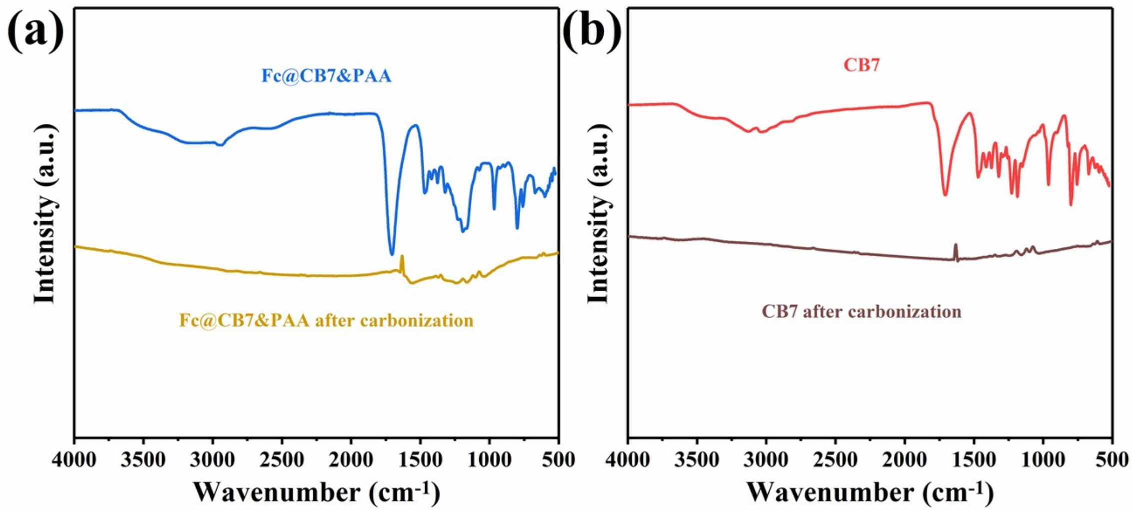

Figure S3. IR spectra of (a) Fc@CB7&PAA and Fc@CB7&PAA after carbonization, (b) CB7 and CB7 after carbonization

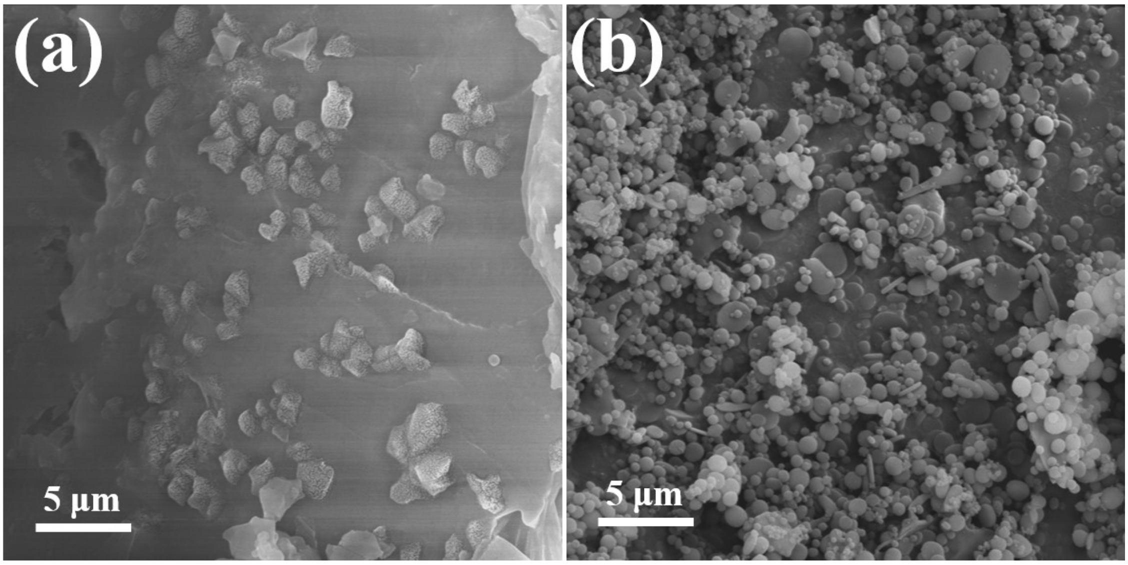

Figure S4. (a)SEM diagram of CB7, (b) SEM diagram of CB7&PAA.

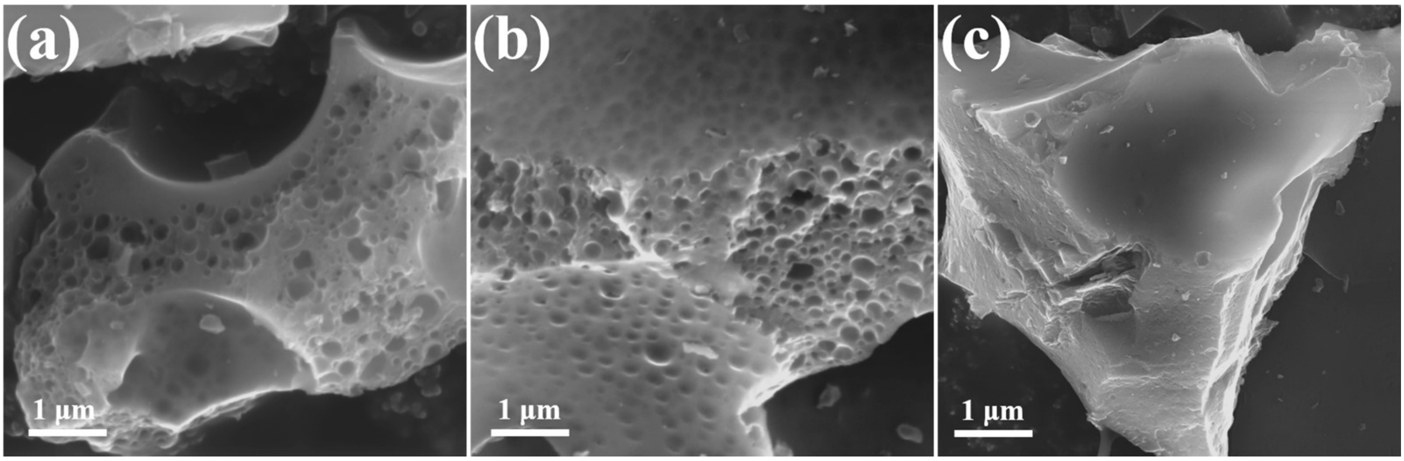

Figure S5. SEM images of (a) Fe_1-N-C, (b) Fe_2-N-C, (c) $Fe_{1,2}$-N-C*.

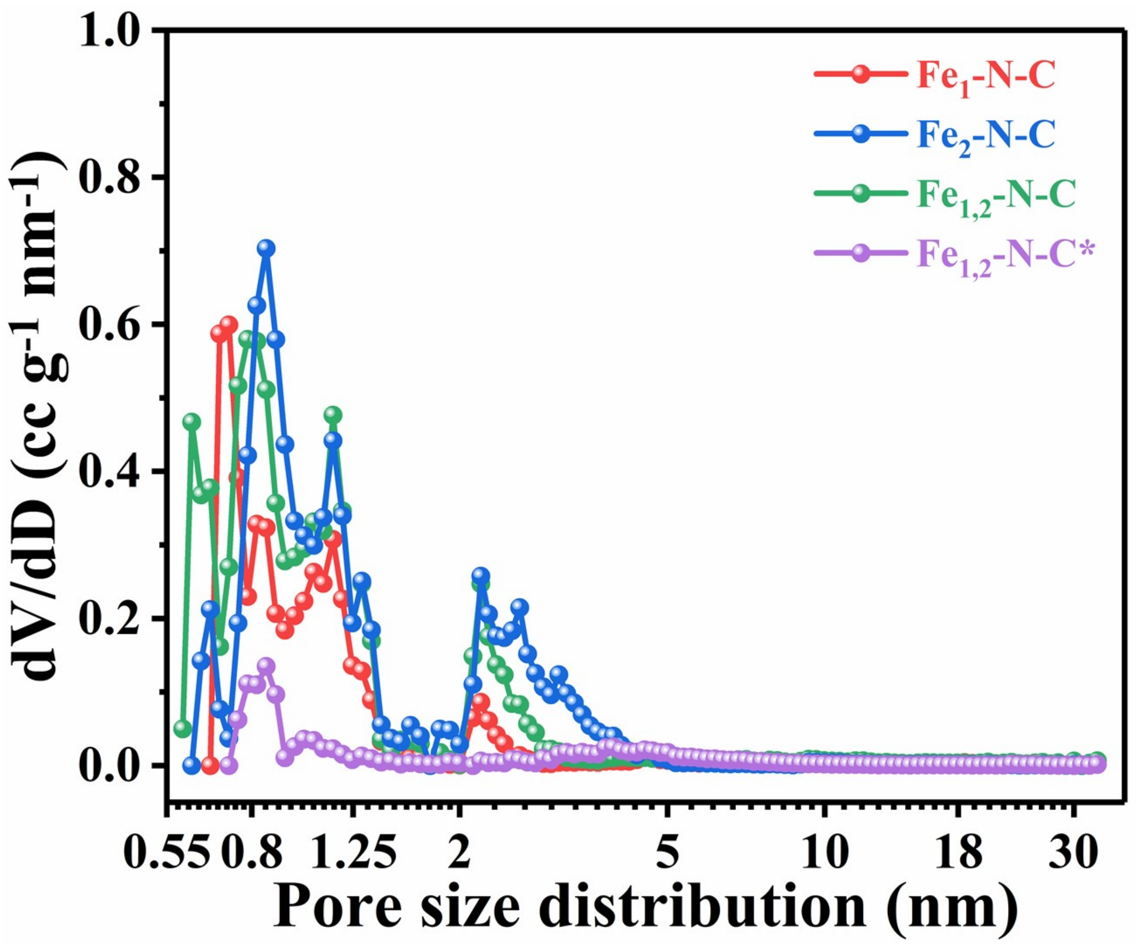

Figure S6. Pore size distribution of Fe_1-N-C, Fe_2-N-C, $Fe_{1,2}$-N-C and $Fe_{1,2}$-N-C*.

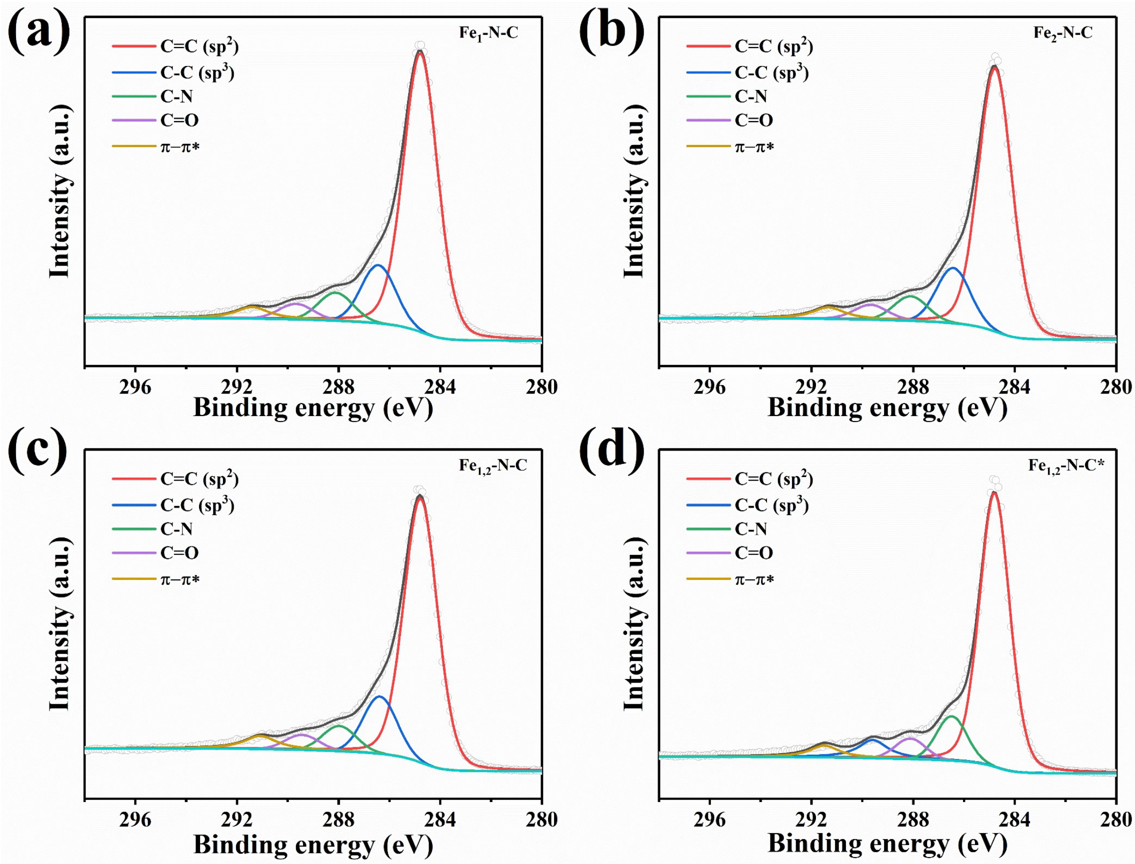

Figure S7. High-resolution C 1s XPS spectra of (a) Fe_1-N-C, (b) Fe_2-N-C, (c) $Fe_{1,2}$-N-C, (d) $Fe_{1,2}$-N-C*.

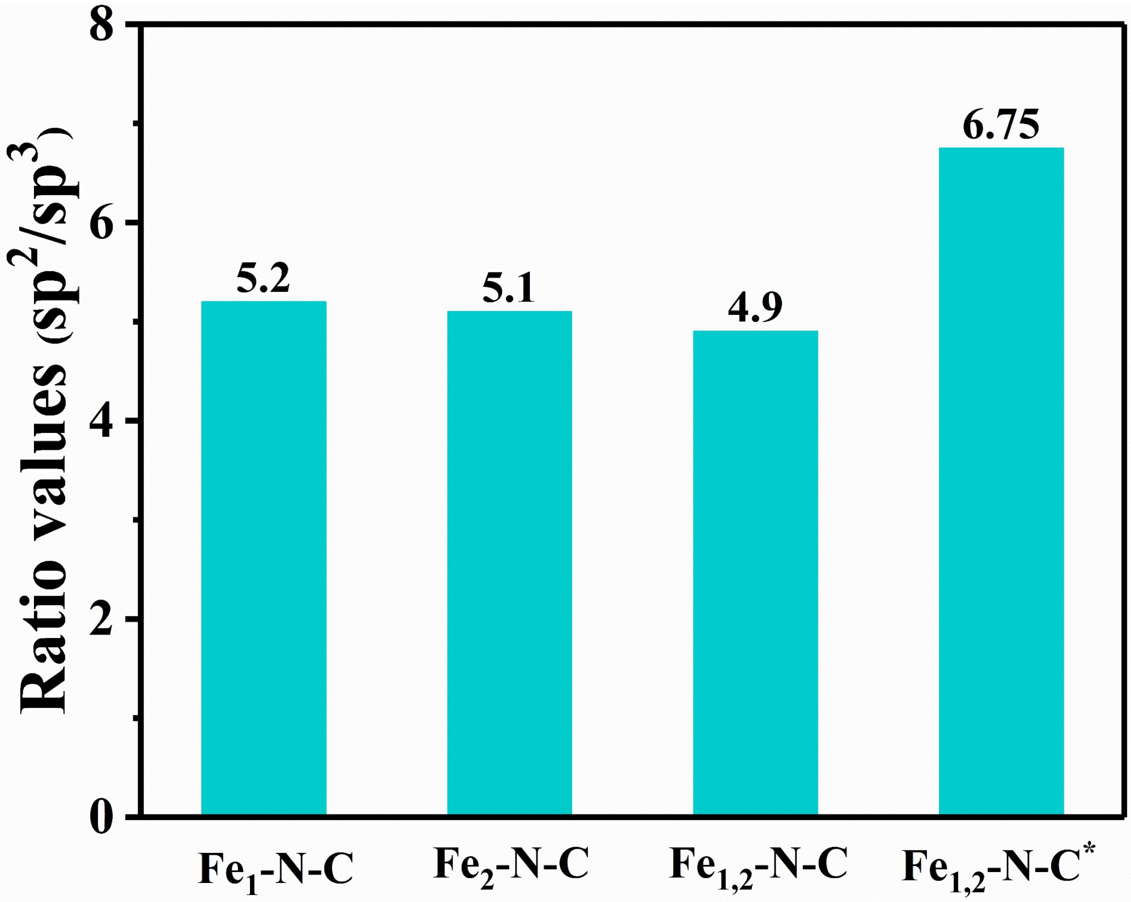

Figure S8. The sp^2/sp^3 ratio values of Fe_1-N-C, Fe_2-N-C, $Fe_{1,2}$-N-C and $Fe_{1,2}$-N-C*.

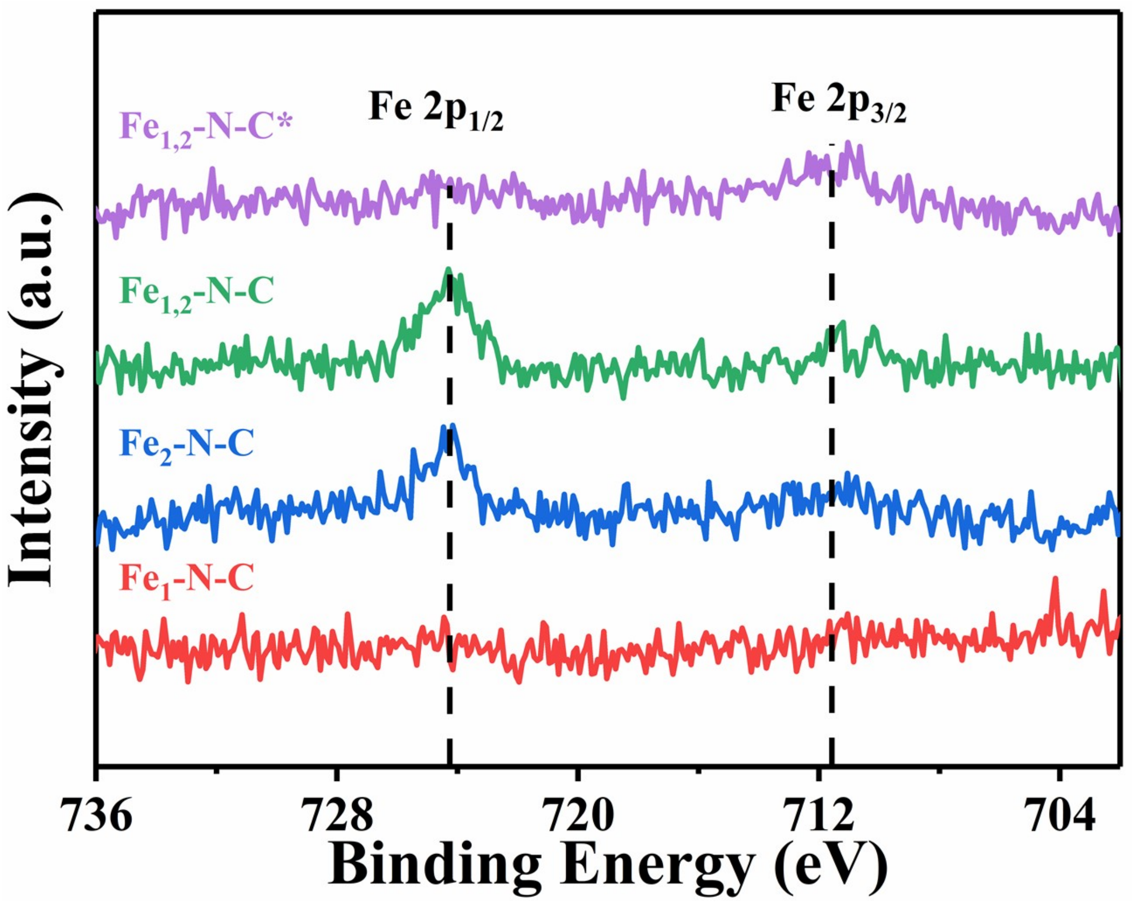

Figure S9. High-resolution Fe 2p XPS spectrum of Fe_1-N-C, Fe_2-N-C, $Fe_{1,2}$-N-C and $Fe_{1,2}$-N-C*.

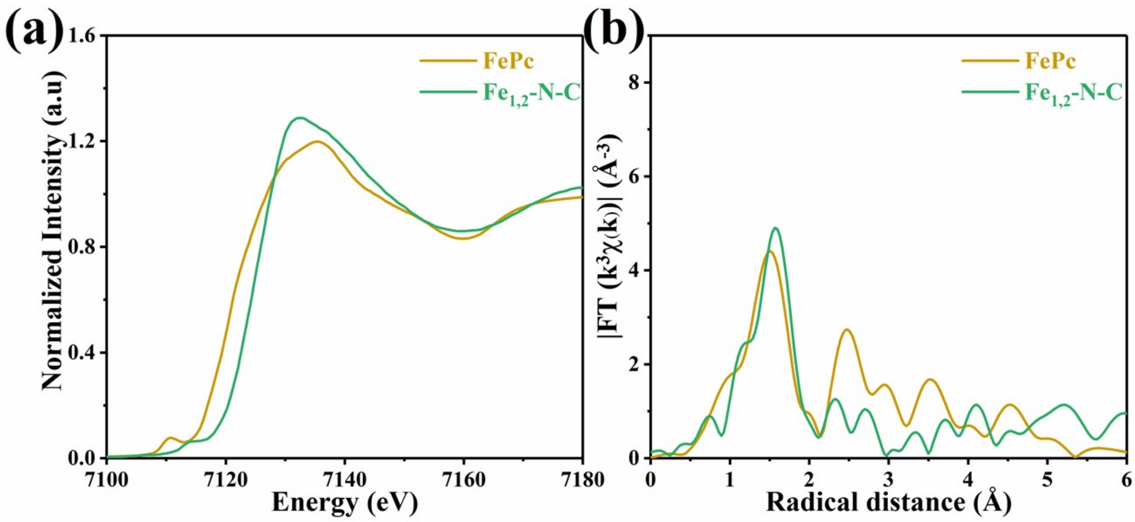

Figure S10. (a) Normalized Fe K-edge XANES spectra and (b) Fourier-transformed k^3-weighted EXAFS spectra of FePc and $Fe_{1,2}$-N-C.

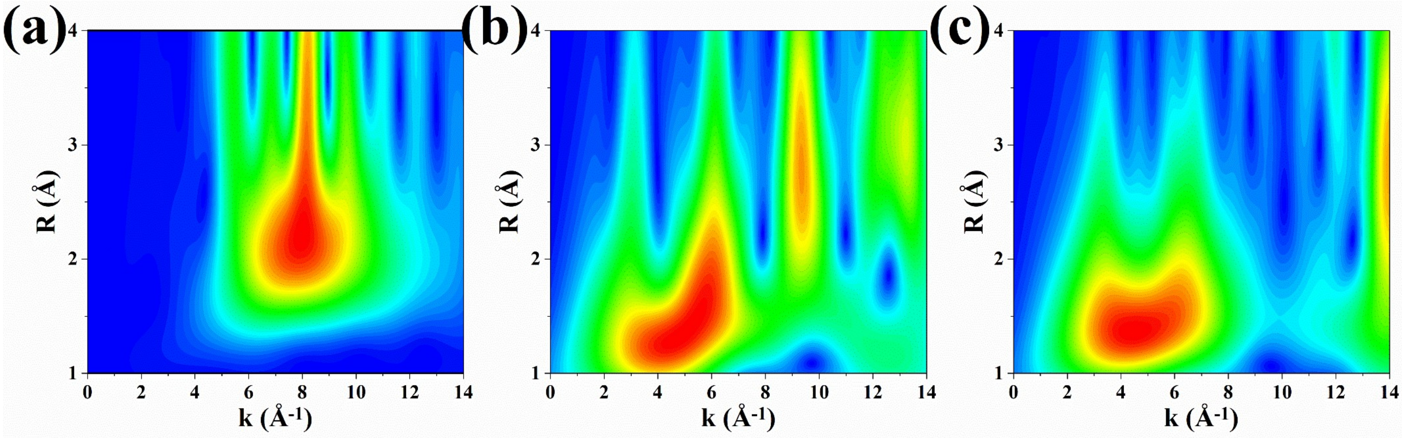

Figure S11. Wavelet transforms for the k^3-weighted Fe K-edge EXAFS signals of (a) Fe foil, (b) FePc, and (c) $Fe_{1,2}$-N-C.

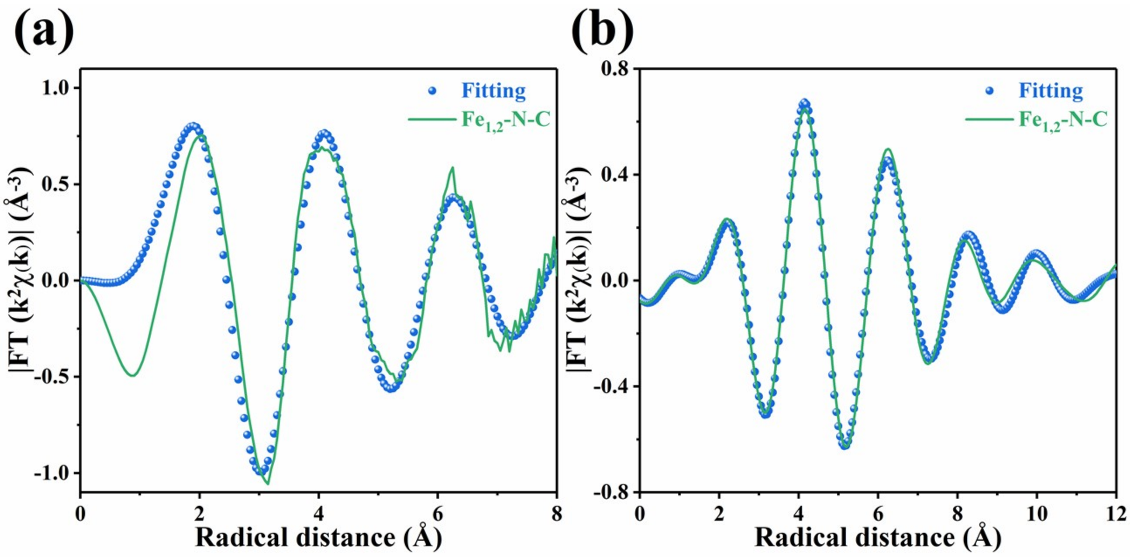

Figure S12. The corresponding FT-EXAFS (a) k-space and (b) q-space fitting curves of $Fe_{1,2}$-N-C.

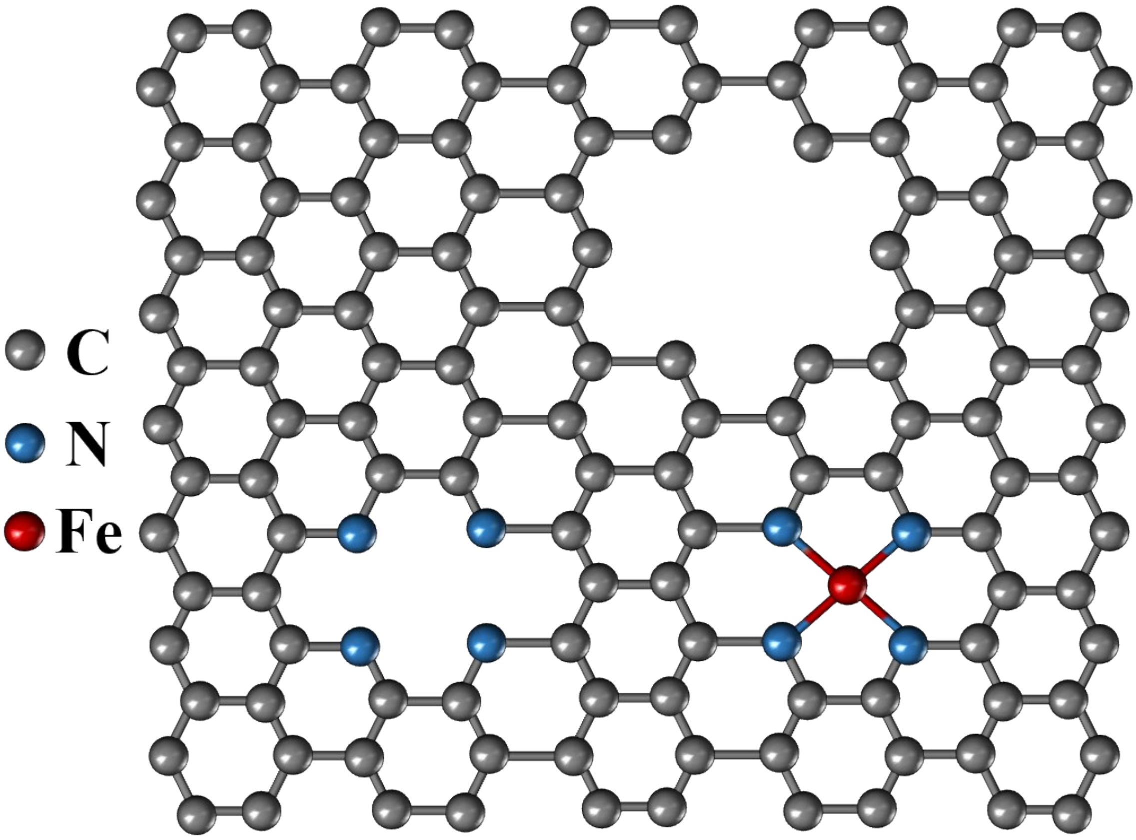

Figure S13. The possible model structure of the active site of $Fe_{1,2}$-N-C.

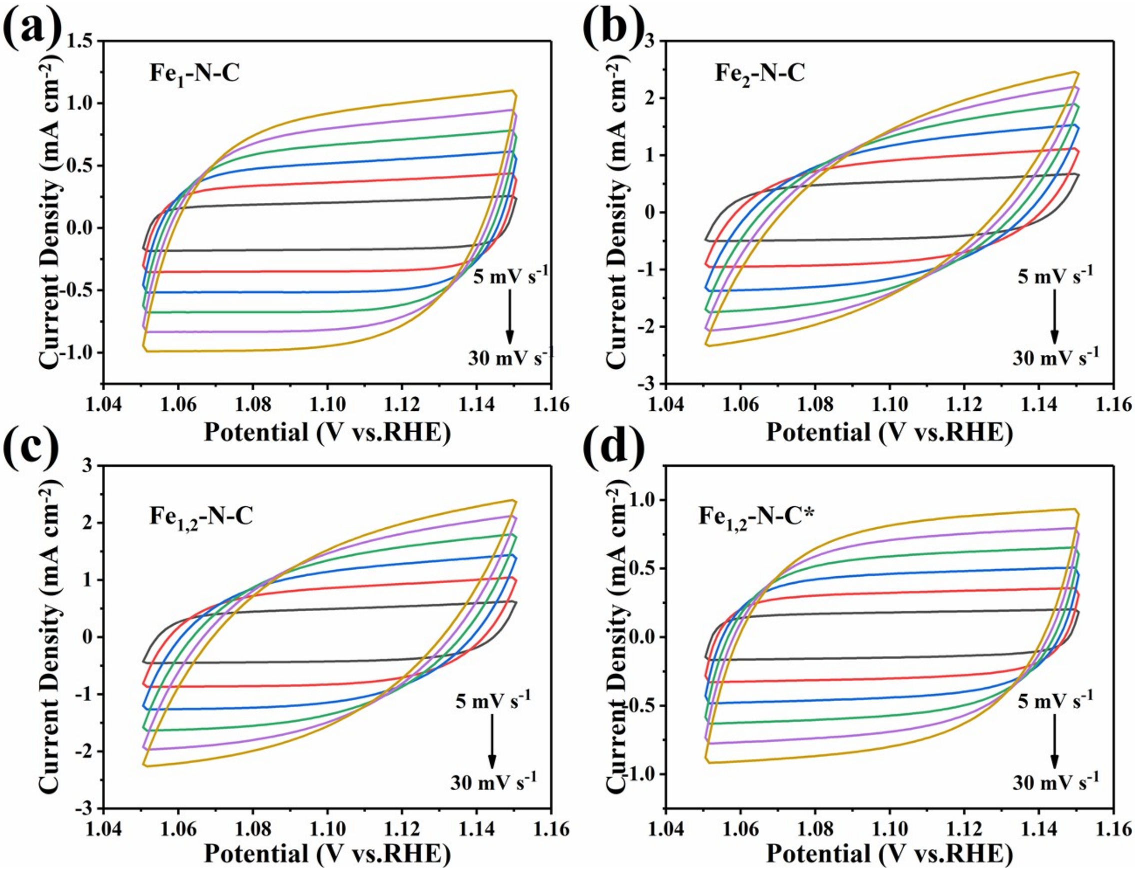

Figure S14. CV curves at various scan rates of (a) Fe_1-N-C, (b) Fe_2-N-C, (c) $Fe_{1,2}$-N-C, (d) $Fe_{1,2}$-N-C*.

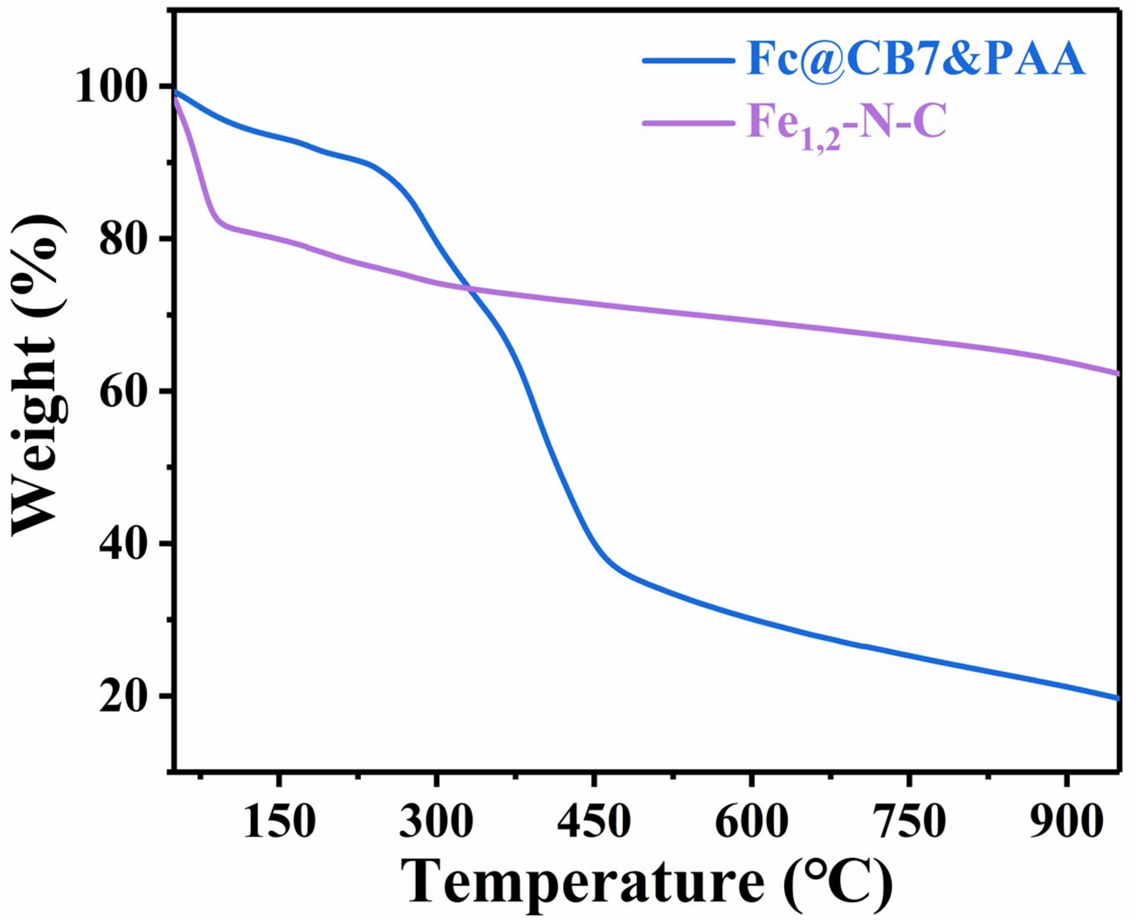

Figure S15. TGA curves (nitrogen atmosphere) for $Fe_{1,2}$-N-C and Fc@CB7&PAA.

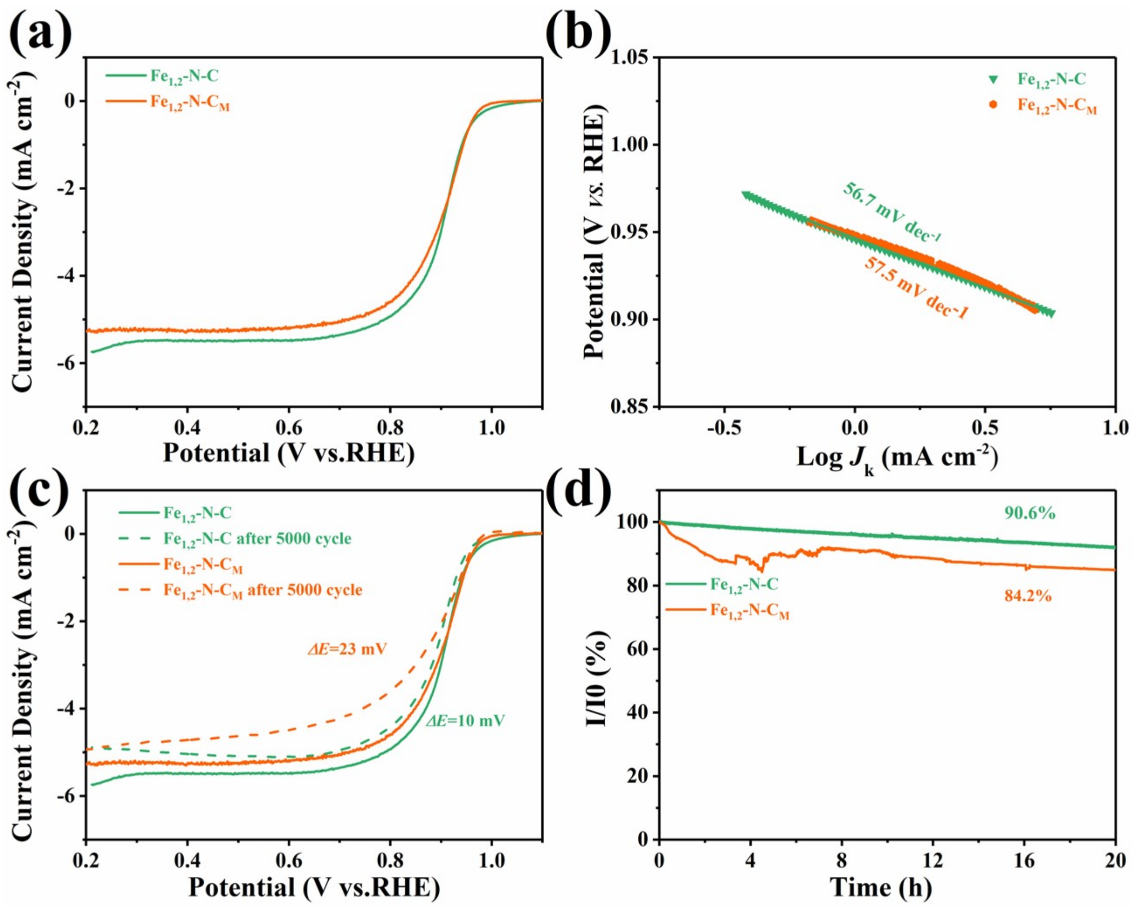

Figure S16. CV curves at various scan rates of (a) Fe_1-N-C, (b) Fe_2-N-C, (c) $Fe_{1,2}$-N-C, (d) $Fe_{1,2}$-N-C*.

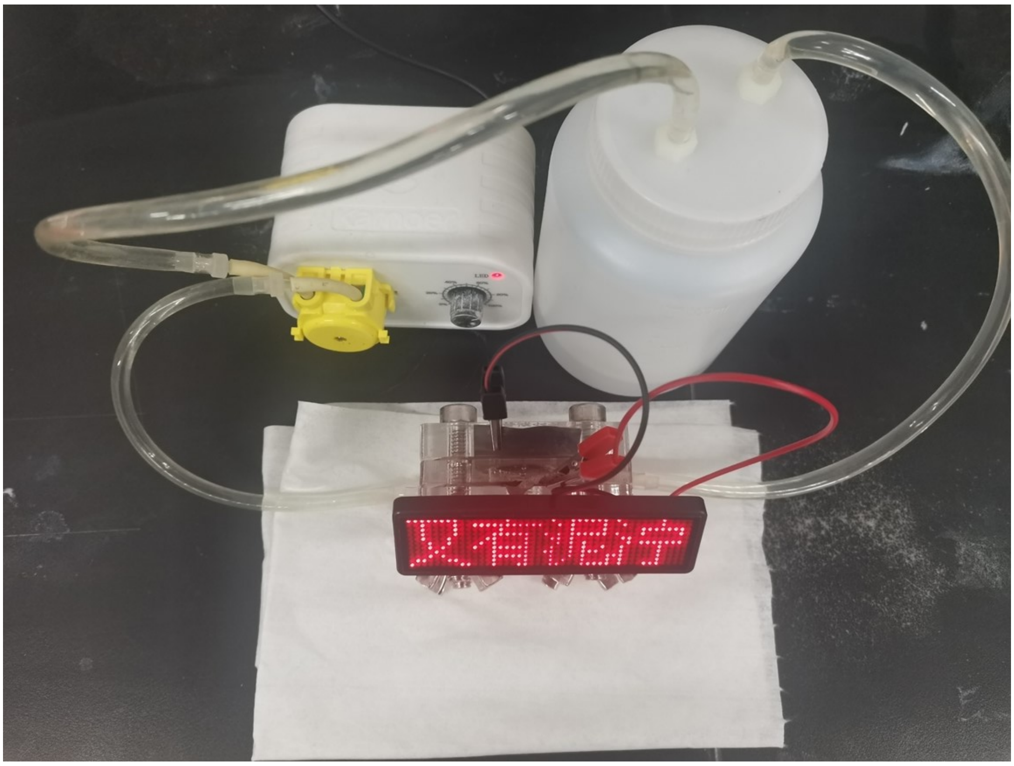

Figure S17. Photograph of the aqueous ZAB with $Fe_{1,2}$-N-C as the air cathode light up a red light-emitting diode (LED) screen.

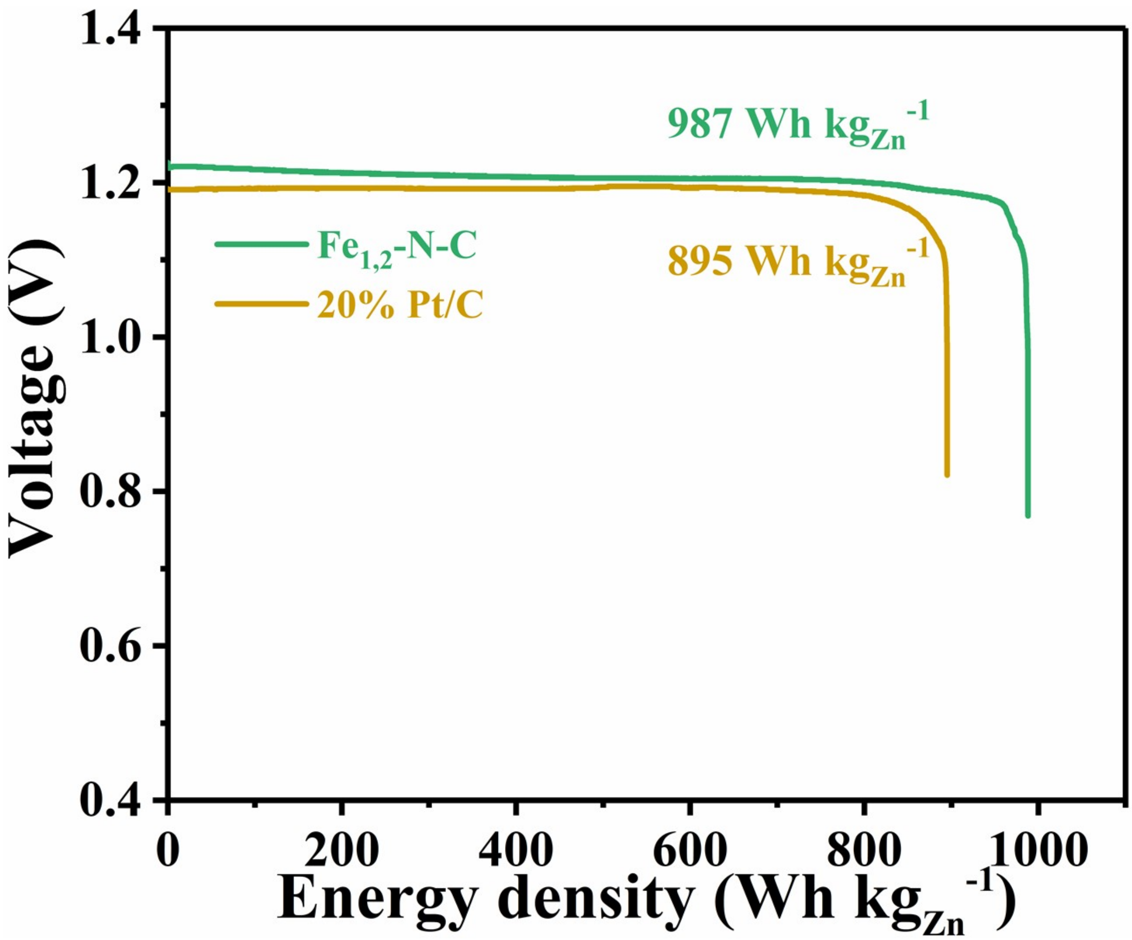

Figure S18. Galvanostatic discharge curves of $Fe_{1,2}$-N-C and 20% Pt/C in aqueous ZABs at a current density of 20 mA cm^{-2}. The specific energy was calculated based on the mass loss of consumed Zn and the average voltage

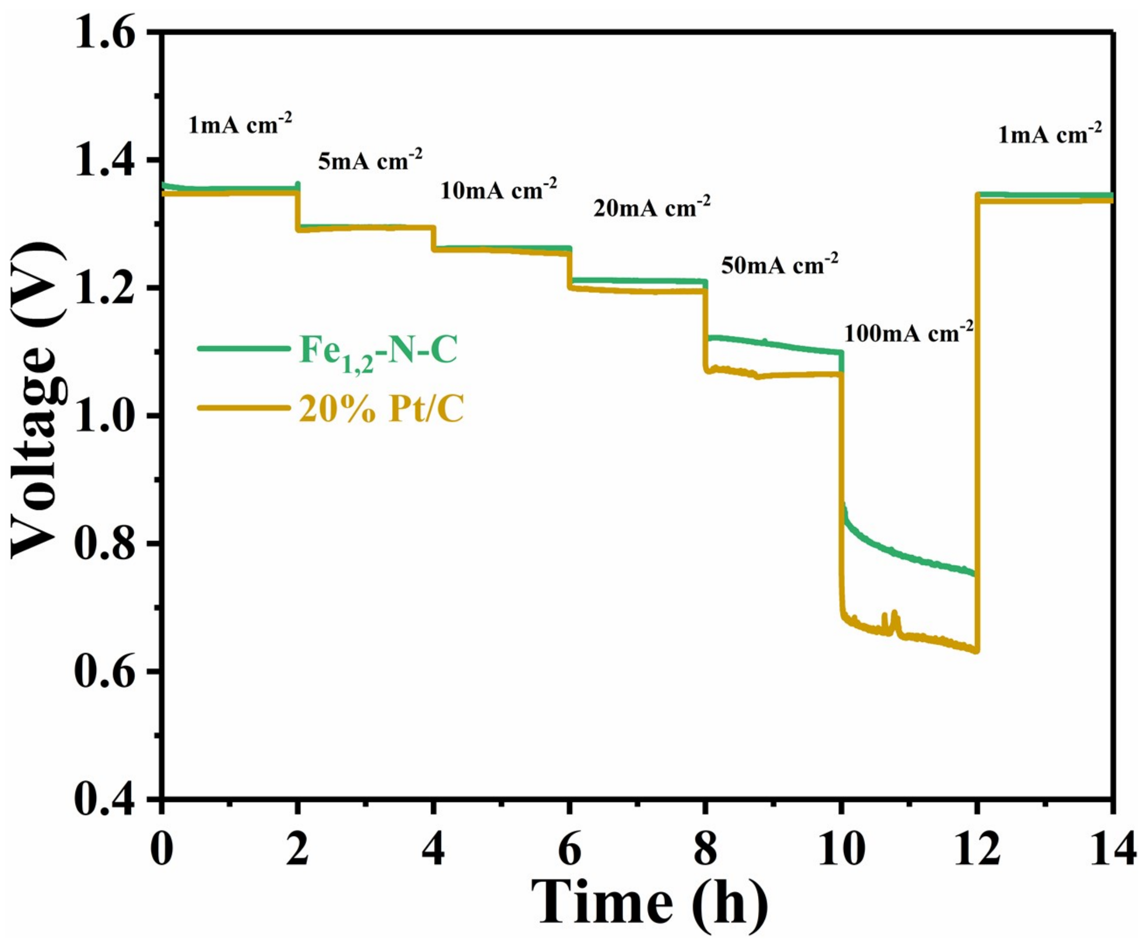

Figure S19. The galvanostatic discharge curves of the aqueous ZABs at various current densities using $Fe_{1,2}$-N-C and 20% Pt/C as air electrodes, respectively.

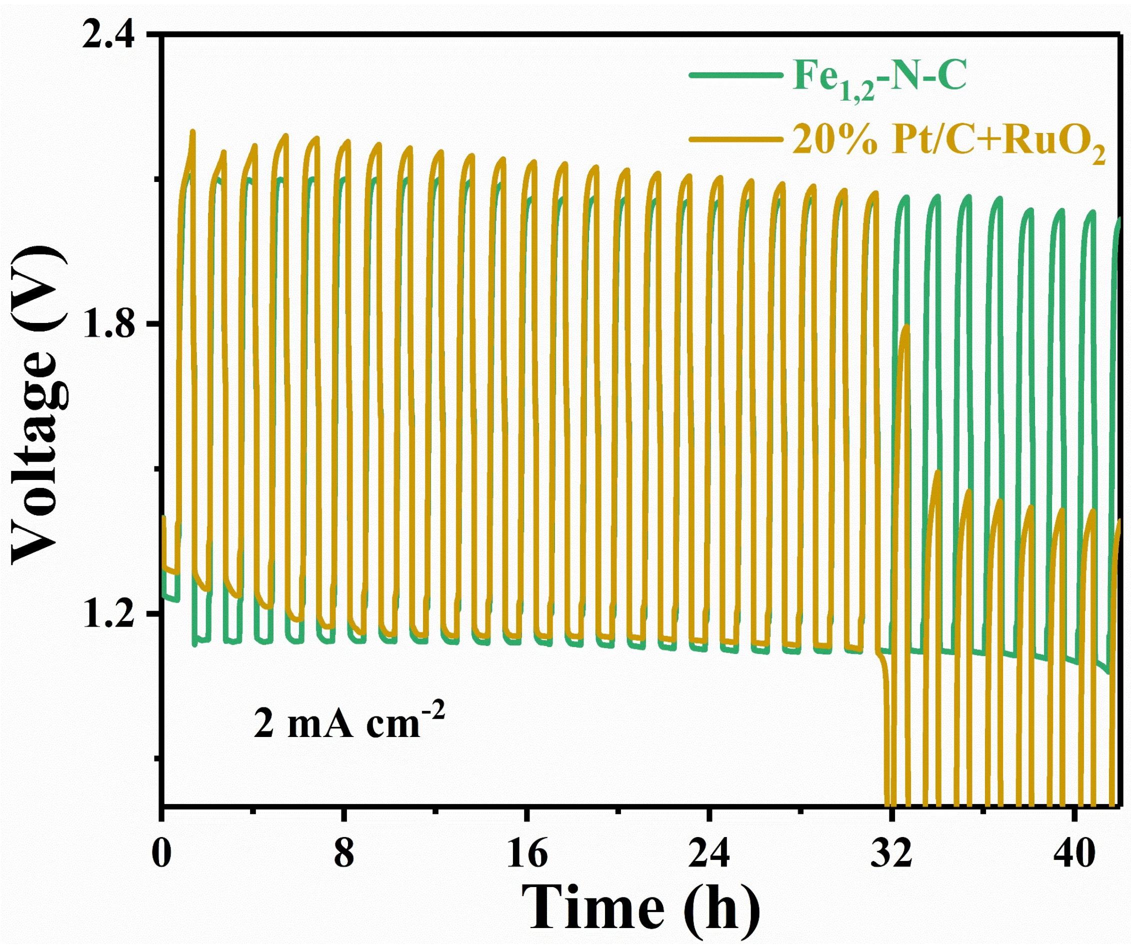

Figure S20. Charge and discharge curve with $Fe_{1,2}$-N-C and 20% Pt/C+RuO_2 as an air electrode.

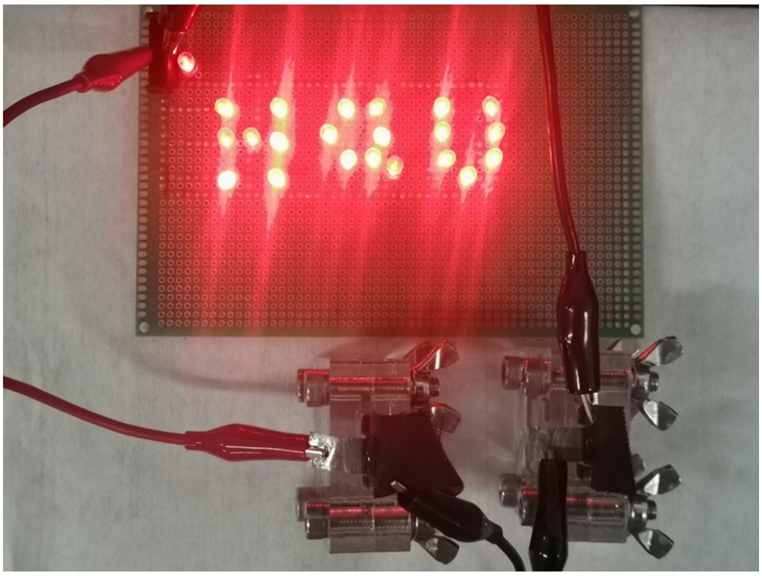

Figure S21. Photograph of the quasi-solid ZAB with $Fe_{1,2}$-N-C as the air cathode light up a red light-emitting diode (LED).

Table S1. The residual Zn contents of Fe_1-N-C, Fe_2-N-C, $Fe_{1,2}$-N-C by ICP-OES

Sample	Zn (weight percentage, %)
Fe_1-N-C	0.04
Fe_2-N-C	0.09
$Fe_{1,2}$-N-C	0.08

Table S2. The The Iron contents of Fe_1-N-C, Fe_2-N-C, $Fe_{1,2}$-N-C, $Fe_{1,2}$-N-C_M by ICP-OES

Sample	Fe (weight percentage, %)
Fe_1-N-C	1.20
Fe_2-N-C	1.27
$Fe_{1,2}$-N-C	2.33
$Fe_{1,2}$-N-C_M	1.13

Table S3. Fitting result of FT-EXAFS curves

Sample	**shell**	**R (Å)**	**N**	**σ^2 ($\times 10^{-3}$ Å^2)**	**R-factor (%)**
Fe foil	Fe-Fe1	2.46	8.0	4.7	0.005
	Fe-Fe2	2.84	6.0	8.2	0.005
FePc	Fe-N	1.97	4.0	6.1	0.022
$Fe_{1,2}$-N-C	Fe-N	2.03	4.0	9.3	0.021

Table S4. Comparison of ORR performance of $Fe_{1,2}$-N-C electrocatalysts with previously reported PGM-free catalysts in O_2-saturated 0.1M KOH.

Electrocatalysts	E_{onset} (V)	$E_{1/2}$ (V)	J_K@0.85V (mA cm^{-2})	J_K@0.9V (mA cm^{-2})	Tafel slope (mV dec^{-1})	Ref.
$Fe_{1,2}$-N-C	1.01	0.91	--	11.28	56.7	**This**
20% Pt/C	0.98	0.89	--	6.68	67.4	**work**
$Fe_{1,2}$-N-C_M	1.00	0.90	--	7.83	57.5	
NPCNF-O	0.98	0.85		--	66.0	1
Fe-SNC-β-CD	1.01	0.90	--	4.10	68.2	2
HPNSC	0.98	0.87	--	--	64.0	3
CoN-PCNS	0.93	0.87	5.7	--	--	4
SC-Fe	--	0.87	--	--	51.3	5
Fe-NHC	0.94	0.89	--	--	53.7	6
FeMnac/Mn-N_4C	1.00	0.90	--	7.71	87.4	7
FeNC-2 M	--	0.897	8.37	--	49	8
Fe-ACSA@NC	1.03	0.90	--	5.61	78	9
β-FeOOH/PNGNs	--	0.883	--	--	83.65	10
Fe-N/P-C-700	0.94	0.867	5.66	--	---	11
FeSA-N-C	1.00	0.90	37.19	--	--	12
FeCo-N-C-700	1.01	0.896	--	--	72	13
Mn-SAS/CN	--	0.91	36.58	--	69	14
S-Cu-ISA/SNC	1.05	0.91	35	--	--	15

Table S5. Comparison of the performance of primary aqueous zinc-air batteries in an alkaline system.

Catalyst	Specific capacity (mAh g_{Zn}^{-1})	Power density (mW cm^{-2})	Energy density (Wh kg_{Zn}^{-1})	j (mA cm^{-2})	Ref.
$Fe_{1,2}$-N-C	816	211.2	987	20	**This work**
20% Pt/C	759	177.0	895	20	
NPCNF-O	726	125.1	--	10	1
HPNSC	799	144.4	957	20	3
Fe-NHC	--	157	907	20	6
FeMnac/Mn-N_4C	720.2	207	--	--	7
Fe-ACSA@NC	--	140	--	--	9
β-FeOOH/PNGNs	722.5	164.5	844.96	10	10
Fe-N/P-C-700	723.6	133.2	--	100	11
FeCo-N-C-700	518	150	--	10	13
Mn-SAS/CN	780	220	--	10	14
S-Cu-ISA/SNC	735	225	--	10	15

Table S6. Comparison of the performance of quasi-solid zinc-air batteries in the alkaline system.

Catalyst	Open circuit (V)	Power density (mW cm^{-2})	Specific capacity (mAh g_{Zn}^{-1})	j (mA cm^{-2})	Ref.
$Fe_{1,2}$-N-C	1.42	73.7	745	2	**This**
20% Pt/C	1.39	73.3	688	2	**work**
FeMnac/Mn-N_4C	1.38	--	--	--	7
FeCo/Se-CNT	1.405	37.5	--	--	16
N/E-HPC-900	1.34	36.2	749	10	17
CNT@POF	1.39	22.3	$<$400	2	18
Fe1/d-CN	1.50	78	--	--	19
Co_3O_4/N-rGO	1.31	--	550	6	20

References

1. F. Qiang, J. Feng, H. Wang, J. Yu, J. Shi, M. Huang, Z. Shi, S. Liu, P. Li and L. Dong, *ACS Catalysis*, 2022, **12**, 4002-4015.
2. C. Chen, H. Li, J. Chen, D. Li, W. Chen, J. Dong, M. Sun and Y. Li, *Energy & Environmental Materials*, 2022, **6**.
3. Y. Cheng, Y. Wang, Q. Wang, Z. Liao, N. Zhang, Y. Guo and Z. Xiang, *Journal of Materials Chemistry A*, 2019, **7**, 9831-9836.
4. Y. Chen, X. Li, W. Liao, L. Qiu, H. Yang, L. Yao and L. Deng, *Journal of Materials Chemistry A*, 2021, **9**, 3398-3408.
5. J. Xie, B. Q. Li, H. J. Peng, Y. W. Song, J. X. Li, Z. W. Zhang and Q. Zhang, *Angewandte Chemie-International Edition*, 2019, **58**, 4963-4967.
6. S. Zhang, W. Yang, Y. Liang, X. Yang, M. Cao and R. Cao, *Applied Catalysis B: Environmental*, 2021, **285**.
7. H. Liu, L. Jiang, J. Khan, X. Wang, J. Xiao, H. Zhang, H. Xie, L. Li, S. Wang and L. Han, *Angewandte Chemie-International Edition*, 2023, **62**, 202214988.
8. C. Shao, J. Hua, Q. Li, Y. Xia, L. Sun, L. Wang and B. Li, *Nano Energy*, 2024, **126**.
9. H. Huang, D. Yu, F. Hu, S. C. Huang, J. Song, H. Y. Chen, L. L. Li and S. Peng, *Angewandte Chemie-International Edition*
2022, **61**, 202116068.
10. Y. Li, J. Huang, X. Hu, L. Bi, P. Cai, J. Jia, G. Chai, S. Wei, L. Dai and Z. Wen, *Advanced Functional Materials*, 2018, **28**.
11. K. Yuan, D. Lutzenkirchen-Hecht, L. Li, L. Shuai, Y. Li, R. Cao, M. Qiu, X. Zhuang, M. K. H. Leung, Y. Chen and U. Scherf, *Journal of the American Chemical Society*, 2020, **142**, 2404-2412.
12. L. Jiao, R. Zhang, G. Wan, W. Yang, X. Wan, H. Zhou, J. Shui, S. H. Yu and H. L. Jiang, *Nature Communications*, 2020, **11**, 2831.
13. X. Duan, S. Ren, N. Pan, M. Zhang and H. Zheng, *Journal of Materials Chemistry A*, 2020, **8**, 9355-9363.
14. X. Han, T. Zhang, W. Chen, B. Dong, G. Meng, L. Zheng, C. Yang, X. Sun, Z. Zhuang, D. Wang, A. Han and J. Liu, *Advanced Energy Materials*, 2020, **11**.
15. H. Shang, X. Zhou, J. Dong, A. Li, X. Zhao, Q. Liu, Y. Lin, J. Pei, Z. Li, Z. Jiang, D. Zhou, L. Zheng, Y. Wang, J. Zhou, Z. Yang, R. Cao, R. Sarangi, T. Sun, X. Yang, X. Zheng, W. Yan, Z. Zhuang, J. Li, W. Chen, D. Wang, J. Zhang and Y. Li, *Nature Communications*, 2020, **11**, 3049.
16. H. Zhang, M. Zhao, H. Liu, S. Shi, Z. Wang, B. Zhang, L. Song, J. Shang, Y. Yang, C. Ma, L. Zheng, Y. Han and W. Huang, *Nano Letters*, 2021, **21**, 2255-2264.
17. X. Peng, L. Zhang, Z. Chen, L. Zhong, D. Zhao, X. Chi, X. Zhao, L. Li, X. Lu, K. Leng, C. Liu, W. Liu, W. Tang and K. P. Loh, *Advanced Materials*, 2019, **31**, 1900341.
18. B.-Q. Li, S.-Y. Zhang, B. Wang, Z.-J. Xia, C. Tang and Q. Zhang, *Energy & Environmental Science*, 2018, **11**, 1723-1729.
19. M. Zhao, H. Liu, H. Zhang, W. Chen, H. Sun, Z. Wang, B. Zhang, L. Song, Y. Yang, C. Ma, Y. Han and W. Huang, *Energy & Environmental Science*, 2021, **14**, 6455-6463.

20. Y. Li, C. Zhong, J. Liu, X. Zeng, S. Qu, X. Han, Y. Deng, W. Hu and J. Lu, *Advanced Materials*, 2018, **30**.